Grain boundary segregation and precipitation in aluminium alloys

de Haas, M.; De Hosson, J.T.M.; Hass, M. de

Published in:
Scripta Materialia

DOI:
10.1016/S1359-6462(00)00577-7

Publication date:
2001

PERGAMON

Scripta mater. 44 (2001) 281–286

Scripta MATERIALIA

www.elsevier.com/locate/scriptamat

GRAIN BOUNDARY SEGREGATION AND PRECIPITATION IN ALUMINIUM ALLOYS

M. de Hass and J.Th.M. De Hosson

Department of Applied Physics, Materials Science Center and Netherlands Institute for Metals Research, University of Groningen, Nijenborgh 4, 9747 AG Groningen, The Netherlands

(Received April 10, 2000)
(Accepted in revised form August 11, 2000)

Keywords: Aluminum alloys; Grain boundaries; Segregation; Transmission electron microscopy

Introduction

The main advantage of aluminium alloys is their high strength to weight ratio and therefore these alloys are considered as a good choice for automotive applications and airframe structure manufacturing. However, the commercial applications may be restricted by poor characteristics such as resistance to stress corrosion cracking, intergranular embrittlement and intergranular fracture. These characteristics depend strongly on the size and distribution of grain boundary precipitates, but also on the width of the precipitate free zone. In this respect, the quench rate is a very important processing parameter. During industrial processing [1] large bars are water quenched after the solution heat treatment. It is obvious that the inner regions of these bars are subjected to slower cooling rates than the outer parts, which will certainly affect grain boundary precipitation during the subsequent ageing treatment.

The intergranular fracture mode mainly consists of microvoid initiation at GB precipitates, growth of voids in the soft PFZ region and final coalescence of the voids. Coarse GB precipitates and wide PFZ attribute to this process [2]. This fracture mode seems to be unaffected by deformation temperature.

Modeling Segregation and Grain Boundary Precipitation during Processing [3,4]

During Quenching

The magnitude of non-equilibrium segregation (NES) is determined, assuming that only diffusion of vacancy-impurity complexes occurs. It simply indicates the change in concentration brought about at the vacancy sink (i.e. the grain boundary) during cooling from temperature T_i to $T_{0.5Tm}$, where T_i is the solution treatment temperature and $T_{0.5Tm}$ is half the melting temperature. This temperature is chosen because it is assumed that very little diffusion will occur below $T_{0.5Tm}$. The quenching is now assumed to be sufficiently fast so that the isolated impurity atoms (non-complexed) cannot move. At the sink the ratio $C_{complexes}$ /$C_{isolatedimp}$ will decrease, whereas this ratio will remain roughly constant in the grain interior where no vacancy sinks exist. The complexes will diffuse down the concentration gradients between the grain centers and grain boundaries in an effort to keep the concentration of complexes equal at all points. Therefore an excess of impurities will be established at the grain boundaries. If it is assumed that during the quench an equilibrium is instantaneously established, corresponding to $T_{0.5Tm}$ on the grain boundary and corresponding to T_i at the grain center, the excess at the grain boundary can be represented as the ratio C_{GB}/C_{Grain}.

PII: S1359-6462(00)00577-7

$$\frac{C_{GB}}{C_{Grain}} = Exp\left(\frac{E_b - E_f}{kT_i} - \frac{E_b - E_f}{kT_{0.5T_m}}\right)\frac{E_b}{E_f} \quad (1)$$

E_f is the thermodynamic free energy of vacancy formation and E_b that of vacancy-impurity binding taken as 1.25 eV and 0.26 eV for Mg (i.e. the rate controlling element) respectively [5,6]. Further relevant equations are given in [3,4].

During Ageing

During ageing, the width of the solute-concentrated layer at the GB stops increasing with time. The diffusion of vacancy-solute complexes down the remaining concentration gradients between the grain center and the GB interface brings the solute towards the grain boundaries. Subsequently, nucleation and growth of grain boundary precipitates takes place. For details see [3,4].

Experimental Procedures

The composition of the AA6061 alloy is 0.97 at% Mg, 0.60 at% Si, 0.14 at% Cu. The alloy was homogenized for 6 hours at 565° C and rolled to 200 μm. Discs with a diameter of 3 mm were punched and a solution heat treatment at 550° C for 25 minutes was given. Subsequently, a water quench was applied and the discs were aged for 3 mins, 1 h, 3 h, 7h, 21.5 h, 50 h and 100 h.

The composition of the AA7050 alloy is 2.7 at% Mg, 2.8 at% Zn and 1.0 at% Cu. The alloy was homogenized for 6 hours at 530° C and rolled to 200 μm. Discs with a diameter of 3 mm were punched and a solution heat treatment at 475° C for 25 minutes was given. Subsequently, a water quench was applied and the discs were aged for 3 mins, 1 h, 3 h, 7 h, 23.5 h, 51 h and 99.5 h. From now on, the samples aged for 3 mins will be referred to as 'as-quenched'. This small ageing time is performed to counteract the deleterious effects of natural ageing [7]. Thin foils for transmission electron microscopy were prepared by using a TENUPOL electropolisher with an electrolyte of 30% nitric acid in methanol at −20° C. The voltage was 20 V.

A JEOL 2010FEG analytical transmission electron microscope with a minimum electron probe size of ~ 0.5 nm and equipped with an EDS detector was used to obtain experimental measurements. Solute enrichment at the GB in the as-quenched sample was measured by placing the electron probe on and at different distances from the grain boundary.

Size measurements were made by tilting the foil so that the length of the grain boundary precipitates was a maximum. For each ageing time, the average length of the ten largest precipitates of three different random high-angle GB's was calculated. The largest precipitates were chosen because of the 2D-projection in which the precipitates appear in TEM. The average inter-distance of the grain boundary precipitates was determined by using four different random high-angle grain boundaries and inter-distances of ten precipitate pairs per boundary. Both the longitudinal (i.e. the direction of precipitate growth) and the transversal inter-distances were measured. Tilting was performed until the inter-distance between the precipitates was largest. At grain boundaries inclined to the surface the transversal inter-distance was calculated using the thickness of the specimen and the 2D-projected width of the GB.

Results

Solute Enrichment at the Grain Boundary after the Water Quench in AA7050

Calculations predict that a 200 μm thick disc of AA7050 at 475° C cools down to the water-temperature of 20° C in less than 0.1 s. However, the samples have to be taken out of the furnace first. The moment

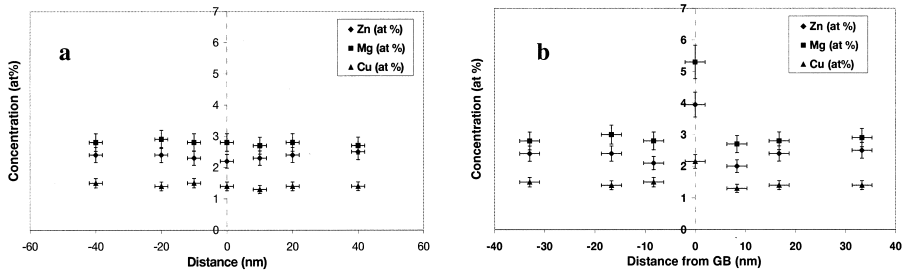

Figure 1. AA7050 solution- heat treated at 475°C and water-quenched. Concentration of Zn, Mg and Cu against distance from the grain boundary. a. Σ9 boundary; b. Random high-angle grain boundary.

that the samples are removed from the furnace is taken as the starting point for the quench and the quench time is estimated to be ~1 s.

Fig 1 shows two composition profiles of as-quenched AA7050. The left profile is of a special GB (Σ9), the right one of a random high angle GB.

Grain Boundary Precipitate Morphology in AA6061 and AA7050

By applying EDS-analysis for composition, the Mg/Si-ratio of most of the grain boundary precipitates in AA6061 was determined to be ~1.3 for all applied ageing times. The structure could only be determined by electron diffraction after the precipitates were sufficiently large (i.e. after 21.5 h of ageing). An HCP-structure (a = 10.60 Å, c = 4.04 Å) was found. All precipitates seem to be lenticular in shape. In AA7050, a phase with a HCP structure (a = 5.32 Å, c = 8.79 Å) nucleates on the grain boundary. This structure is very similar to that of $MgZn_2$. However, EDS-analysis also reveals Cu next to Mg and Zn. This could be an indication that $Mg(Zn,Cu)_2$ has formed in which some of the Zn is replaced by Cu.

Grain Boundary Precipitate Nucleation and Growth in AA6061 and AA7050

Both as-quenched AA6061 (Fig. 2a) and AA7050 alloys show no obvious grain boundary precipitation. This supports the fact that nucleation only occurs during ageing and not during the rapid water quenching. For all other applied ageing times grain boundary precipitation could be observed (TEM micrographs of AA6061 in Figs. 2b-2f), except for the special grain boundaries and the grain boundaries with a misorientation angle below ~3°. Above observations support the theory that there is less or no segregation towards special and low-angle (<3°) grain boundaries.

As they are the largest in number, only the length of the precipitates with Mg/Si ~1.33 in AA6061 is measured for different ageing times and compared to the predicted values. Input parameters of the model for AA6061 are given in the appendix.

The results are depicted in Fig. 3. Experimental and theoretical values for the length of $Mg(Zn,Cu)_2$ precipitates in AA7050 are depicted in Fig. 4 for comparison.

The longitudinal and transversal distances between two separate GB precipitates in AA6061 are measured for increasing ageing times. The experimental values are compared with the modeled ones and shown in Fig. 5.

Discussion

As can be seen from Fig. 1 there is no visible segregation towards the Σ9 boundary of AA7050. The measured enrichment factor of Mg for the random high-angle grain boundary is ~1.8. This factor is far

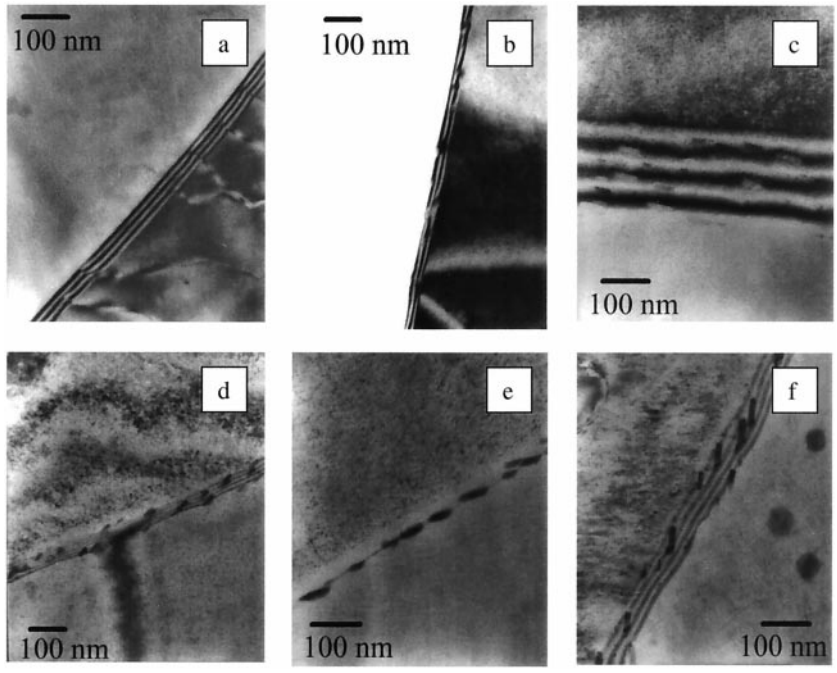

Figure 2. Grain boundaries of AA6061 aged for different times at 160°C. a. 3 mins; b. 1 h; c. 3 h; d. 21.5 h; e. 50 h; f. 100 h.

lower than the predicted value of 35. The predicted width of the solute-concentrated layer for a quench time of 2 s is 1.4 nm. The probe size is about 1 nm which is entirely within the solute concentrated layer (SCL). Etching of the grain boundary during sample preparation may be an explanation for the discrepancy in enrichment factor. As a consequence, the probed area of the grain boundary may then lie deeper in the sample, which yields an inaccurate composition profile because of much larger background signal from surrounding Al. A similar discrepancy was found for AA6061. Measured enrichments at the GB can thus only be interpreted qualitatively.

Structure (after 21.5 h of ageing) and Mg/Si-ratio of the GB precipitates in AA6061 correspond very well to the Q-phase ($Cu_2Mg_8Si_6Al_5$). However, the Cu-content is lower than the stoichiometric value, especially at small ageing times. This may be explained by the β'-phase (Mg/Si-ratio $\sim$1.3, HCP a = 7.05 Å, c = 4.05 Å, no Cu) preceding the Q-phase [8]. For the model, the molar volume of the β'-phase is used.

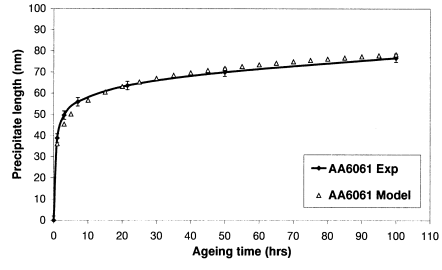

Figure 3. GB precipitate length vs. ageing time at 160°C in AA6061.

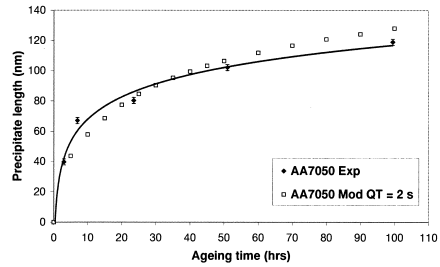

Figure 4. GB precipitate length vs. ageing time at 160°C in AA7050.

As shown in Fig. 3, the calculated GB precipitate lengths for AA6061 are in very good agreement with their experimental counterparts. Fig. 4 clearly shows the faster growth rate of GB precipitates in AA7050 with respect to AA6061. This can be explained by the rate-controlling element in the precipitation reaction which is Mg (the element with the lowest diffusivity at 160° C [7]). For formation of $Mg(Zn,Cu)_2$ less Mg is needed than for formation of β'. The predicted values for AA7050 using a quench time of 2 s are in fair agreement with experimental values.

Fig. 5 shows that for AA6061 subjected to a quench time of 1 s, the calculated inter-distances are in between the experimentally determined longitudinal and transversal inter-distances. This may be explained by the model assuming a square collector-plate, from which the inter-distance is derived by taking the square root of its area. However, the real collector-plates are rectangular in shape, because the precipitate grows faster in the longitudinal direction. The measured longitudinal inter-distance may thus be larger than the value predicted by a square collector-plate model. The transversal inter-distance is shorter than the predicted value, so that the areas of the square (model) and rectangular (experimental) collector plates are comparable.

The grain boundary energy used as input parameter for the model is 0.41 J m^{-2} [9]. This is typical value for the energy of random high-angle grain boundaries in Al. The model is very sensitive on this parameter. The precipitate growth rate and inter-distance both increase with grain boundary energy [10]. Strictly speaking, the model should thus be verified for different misorientations against experimental findings.

Conclusions

- The solute enrichment at the grain boundary determined by TEM with a nanoprobe can only be understood qualitatively.
- EDS-analysis in combination with electron diffraction proves that precipitates with a Mg/Si-ratio of ~1.3 and a structure similar to the Q-phase (at larger ageing times) are present at the grain boundaries

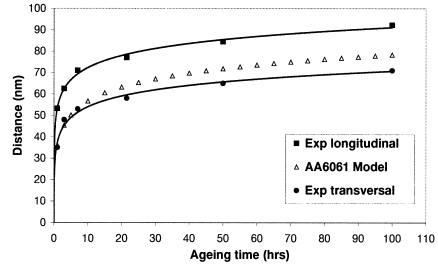

Figure 5. GB precipitate interdistance vs. ageing time at 160°C in AA6061.

of AA6061. The Cu-content is lower than the stoichiometric value, which may indicate that the Q-phase is preceded by the β'-phase.

- The model originally developed for 7XXX-series aluminium alloys is applied to AA6061 and AA7050. Predicted values of the GB precipitate growth are in fair agreement with experimental ones. Calculated inter-distances are in between measured longitudinal and transversal inter-distances. This is explained by the model assuming a square collector plate while a rectangular shape is expected.

Acknowledgments

The authors are indebted to Corus R&D for supplying the material.

References

1. T. Sheppard, Extrusion of Aluminium Alloys, Kluwer Academic Publishers, Dordrecht (1999).
2. G. Itoh, M. Kanno, T. Hagiwara, and T. Sakamoto, Acta Mater. 47, 3799 (1999).
3. H. Jiang and R. G. Faulkner, Acta Mater. 44, 1857 (1996).
4. H. Jiang and R. G. Faulkner, Acta Mater. 44, 1865 (1996).
5. R. G. Faulkner and H. Jiang, Mater. Sci. Technol. 9, 665 (1993).
6. R. G. Faulkner, Mater. Sci. Technol. 1, 442 (1985).
7. L. Zhen, S. B. Kang, and H. W. Kim, Mater. Sci. Technol. 13, 905 (1997).
8. A. Perovic, D. D. Perovic, and G. C. Weatherly, Scripta Mater. 41, 703 (1999).
9. D. A. Porter and K. E. Easterling, Phase Transformations in Metals and Alloys, Chapman and Hall, London (1990).
10. M. A. Cantrell and G. J. Shiflet, Mater. Res. Soc. Symp. Proc. 319, 357 (1994).
11. L. F. Mondolfo, Aluminium Alloys, Structure and Properties, Butterworth, London (1979).
12. R. C. Dorward and C. Bouvier, Mater. Sci. Eng. A254, 33 (1998) (For solubility product equation).

Appendix

Input Parameters for the Grain Boundary Precipitation Model for the Case of an AA6061 Alloy

Parameter	Value	Unit
Molar volume of precipitate phase V_θ	$2.00 \cdot 10^5$ [11]	M^3
Atomic fraction of solute in the nucleus phase X_θ (i.e. of Mg)	0.57	
Solution heat treatment temperature T_i	803	°K
Ageing temperature T_a	433	°K
Concentration of solute in the matrix Cg	0.97	At%
Concentration of solute at the grain boundary Xb	99.7	At%
Enthalpy of solution per mole in solubility product equation ΔH	$1.67 \cdot 10^5$ [12]	J mol^{-1}
Entropy term in solubility product equation S	23.8 [12]	
Precipitate matrix interfacial energy per unit area γ_{ab}	0.32	J m^{-2}
GB width within which the solute diffusion is GB diffusion controlled	$1 \cdot 10^{-10}$ [3,4]	m
Grain boundary energy γ_{gb}	0.41 [9]	J m^{-2}
Molar volume of the matrix phase	$1.004 \cdot 10^{-5}$ [11]	m^3
Ratio between nr. of moles of the non-rate controlling element and moles of the rate-controlling element in precipiate phase	0.75	
Concentration of the non-rate controlling element in matrix (i.e. Si)	0.6	At%
Width of the solute-concentrated layer (at a quench time of 1 s)	$1.44 \cdot 10^{-9}$	m
Width of the solute-depleted layer (at q quench time of 1 s)	$1.47 \cdot 10^{-7}$	m
Vacancy formation energy E_f	1.25	eV
Vacancy-impurity binding energy E_b	0.26	eV